Cement Paste Morphologies and effective diffusivity: using the Lattice Boltzmann Method

E Walther, M Bogdan, R Bennacer, C Desa

Cement Paste Morphologies and effective diffusivity: using the Lattice Boltzmann Method

E. Walther, M. Bogdan, R. Bennacer, C. Desa

LMT-Cachan UMR 8535
61, avenue du Président Wilson
94230 Cachan, FRANCE

{walther, bogdan, bennacer, desa}@lmt.ens-cachan.fr

ABSTRACT. *A novel explicit modeling framework based upon correlated Random Field and Level-Set methods is presented and applied to cement paste hydration. Focus is then made on effective diffusive properties prediction through numerical homogenization, using the Lattice Boltzmann Method (LBM), exploring the stability limits and performance of this method for heterogeneous media.*

RÉSUMÉ. *Une méthode originale de création de morphologies de pâtes de ciment en cours d'hydratation à l'aide d'excursions de champs aléatoires corrélés est introduite. On présente ensuite le calcul des propriétés diffusives effectives homogénéisées de ces pâtes à l'aide de la Méthode de Boltzmann sur gaz réseau, les limites de stabilité et de performances associées à cette méthode pour les matériaux hétérogènes, ainsi qu'une application aux pâtes de ciment en cours d'hydratation*

KEYWORDS: *morphology, correlated random fields, level-set method, cement paste, diffusivity, Lattice Boltzmann*

MOTS-CLÉS : *morphologies, champs aléatoires corrélés, méthodes level-set, pâte de ciment, diffusivité, LBM*

1. Introduction

Understanding and modeling cement based materials has always been a great challenge towards numerous issues, such as durability assessments or effective properties predictions. In this paper an original attempt to model cement paste microstructure is presented, along with an original numerical framework.

First, an original morphological tool is introduced, based upon level-set methods applied to Correlated Random Fields (hereafter CRFs) (Roubin *et al.* (2015)). Unlike most of the existing models, such tools allow to yield "random" morphologies, with targeted volume / surface area fractions. Furthermore, this method allows the control of the entire morphology through a reduced set of parameters, and their evolution is driven by a unique one. In opposition to "particular" models (*e.g.* HYMOSTRUC, van Breugel (1991)) where a set of three parameters are needed to describe every inclusion (in 2D), or "voxelized" models (CEMHYD, Bentz & Garboczi *et al.* (1993)) where local rules governing the evolution through time ; here a unique threshold will control the entire morphology. This framework is applied at the cement paste scale, in 2D, in order to yield morphologies of hydrating cement paste.

The Lattice Boltzmann Method (LBM) provides a simple way to simulate transport phenomena in heterogeneous media such as cement paste (*e.g* the 3D modelling of Zhang *et al.* (2011)). A regular mesh defined once only allows for a simple implementation and its explicit formulation makes it attractive for the simulation of evolving geometries at different time steps, which is the final aim of this study. The parallelization capacity of the LBM also implies a competitive computational cost time compare to traditional numerical methods. This aspect is of particular interest for variability studies: given the statistical CRF-based reconstruction of cementitious material, a high number of simulations may be required for variability studies, such as presented in the final application of this work, which is the extension of the proof of concept provided in Walther *et al.* (2014).

Due to a higher percolation effects through pore connectivity in three dimensions, the two-dimensional calculation of effective diffusivity is indeed less relevant in the case open-cell porosity, however the originality of this work – compared to the extensive approach of Zhang *et al.* (2011) and Zhang *et al.* (2012) – relies on the stability analysis of the LBM as well as in the statistical determination of the equivalent diffusivity, based on numerous calculations of independently generated morphologies as in Roubin *et al.* (2014). Furthermore, this work is to be considered as a validation of the in-house developed LBM code and will be extended to three dimensions in the future.

2. Morphology creation and description

In this first section a morphological framework allowing to easily yield complex morphologies is presented, after Roubin *et al.* (2015) and Bogdan *et al.* (2014). A simplified hydration model is then introduced, and when combined with the morphological yielding process, it allows to generate hydrating cement paste morphologies.

2.1. *Correlated Random Fields and Level-set methods*

The presented morphological framework is based upon Gaussian CRFs thresholding. Those particular random fields are chosen because they can be described with very few parameters: a correlation length L_c, a variance σ and an underlying correlation function. They represent respectively the average width and height of the peaks / valley on Figure 1(a). Lastly the mean value of the RF might be added, but in the following zero mean Gaussian CRFs are used.

Within this work, those CRFs are considered as random functions: $\gamma(\boldsymbol{x}, \omega) = M \in \mathbb{R}^2 \rightarrow \mathbb{R}$, where M is a two dimensions Euclidean space, $\boldsymbol{x}$ is the space variable, and ω the random variable. Thus, the CRFs are defined over a square of size T, with values in $\mathbb{R}$. An excursion A_u of such a function is defined by "the set of points where the values of γ are above a given threshold u", as presented in Equation [1].

$$A_u \equiv A_u(\gamma, M) = \{\boldsymbol{x} \in M | \gamma(\boldsymbol{x}, \omega) \geq u\} \tag{1}$$

An example is shown on Figure 1. On the left side, a realization γ of a CRF over a square is presented, and on the right side the thresholding with the yielded excursion beneath.

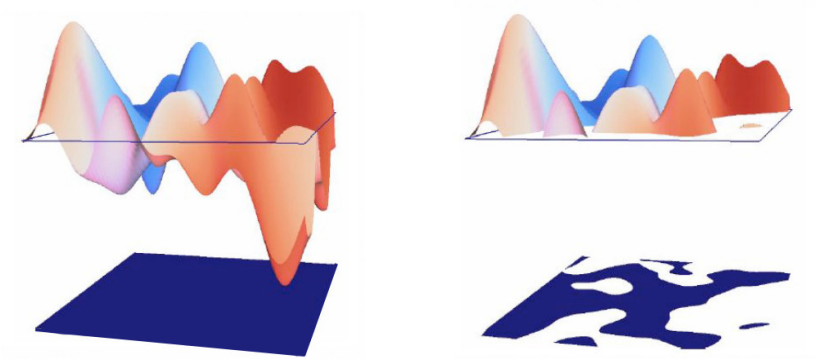

(a) 2D RF realization (b) 2D excursion

Figure 1. *CRF realization, thresholding, and excursion*

The key point in using this framework lies in the work of Adler (2008). It establishes a probabilistic link between the CRFs' quantities (L_c and σ) and the threshold value (u) on one side, and the geometrical and topological quantities of the excursion sets on the other side (System [2], in the general 3D case, V being the volume fraction, S the surface area, and EC the Euler's characteristic that can be seen as a measure of the connectivity). It is thus possible, for a given threshold, to access statistical information about the surface area fraction, the average size of the inclusions, and to a measure of the connectivity for a realization of such morphologies. The predictions are never perfect since the System [2] is only made in terms of expectancies. This link makes this method very powerful, since it is possible to generate morphologies with

a chosen surface area, or a given inclusion size, and then make them evolve through a unique parameter, the threshold. For more details about the probabilistic link and the explicit formulae (functions f, g, and h in System [2]), the reader is referred to Adler (2008) and Roubin *et al.*(2015).

$$\mathbb{E}\{V\} = f(\sigma, L_c) \tag{2a}$$

$$\mathbb{E}\{S\} = g(\sigma, L_c, u) \tag{2b}$$

$$\mathbb{E}\{EC\} = h(\sigma, L_c, u) \tag{2c}$$

In the following this process is used to yield cement paste morphologies, and thus numerous phases has to be represented. The same way a threshold is able to separate a CRF in two parts ; two thresholds yield three phase morphologies, with a new phase "concentric" to the initial inclusions (see Figure 2(c) and 2(d)).

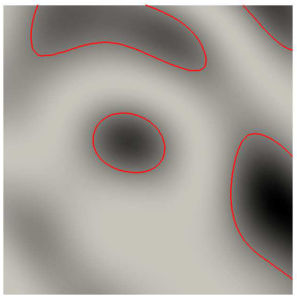

(a) One CRF realization, and the threshold u

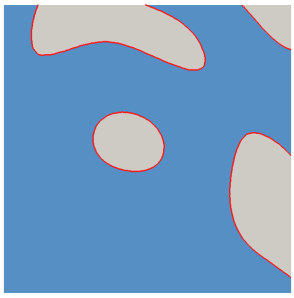

(b) Initial morphology: cement grains and water

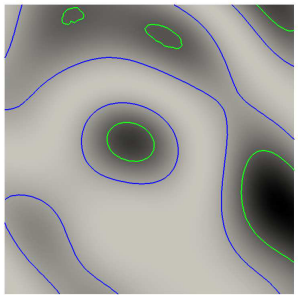

(c) Same CRF realization, with two thresholds: $v \geq u$, and $w \leq u$

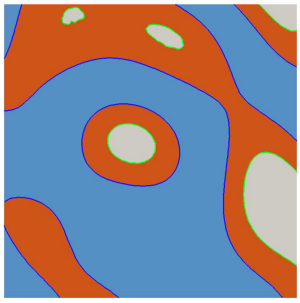

(d) Cement hydration: cement grains, water, and hydrates

Figure 2. *From the RF creation to cement paste morphology yielding - grey: unreacted cement; blue: water; orange: hydration products*

2.2. *Cement pastes hydration: a simplified model*

In order to describe cement paste in hydrated states as well as during hydration, a model is needed to describe their evolution. In a first approximation, the Powers model is implemented (Powers and Brownyard, 1947) for its simplicity (few phases considered in the reactants as well as for the new hydrates, and a macroscopic description of the phases volume fraction evolutions).

Usually, this model considers five volume fractions: anhydrous cement, hydration products, gel water, free water and chemical shrinkage. It has been chosen to use only three for this first application, taking into account only anhydrous cement, hydration products (including gel water) and free water. A more detailed description of the cement paste is possible, but would require a more advanced hydration model (*e.g.* Jennings & Tennis (1994) with each hydrate treated separately). The chemical shrinkage is also neglected in this first implementation, and its volume fraction is allocated to porosity (*i.e.* to the free water phase).

Thus, the overall description is given by System [3]:

$$p = \frac{w/c}{w/c + \rho_w/\rho_c} \tag{3a}$$

$$V_{\text{anh}} = (1-p)(1-\xi) \tag{3b}$$

$$V_{\text{h}} = 2.12(1-p)\xi \tag{3c}$$

$$V_{\text{w}} = 1 - V_{anh} - V_{hyd} \tag{3d}$$

where p is the initial porosity, ξ the hydration degree, and V_{anh}, V_{h} , V_{w} respectively the volume fractions of anhydrous cement, hydration products and water. An example is given Figure 3.

Remark: The simplicity of the hydration description through a unique parameter (the hydration degree ξ) is reminded, as its morphological description through a set of two threshold governing the whole evolution of the microstructures. From a practical point of view, we will consider the following:

– The initial porosity p give us the **initial surface area** (volume fraction) of the cement grains in **the fresh cement paste**,

– the evolution of **the three phases**, and thus **two threshold**, is governed by **a unique parameter**.

– A **maximal hydration degree** is considered – ξ_{max} (not developed here) – to undermine the strong hydration model simplifications.

For more information about level-set methods applied to hydration modeling, and the extension to three dimensional simulations please refer to Bogdan *et al.* (2014). It is shown that the particle size distribution of the anhydrous cement is taken into account (using unions of excursion sets with various correlation lengths, somewhat visible on Figure 3, with various inclusion sizes), as well as more developed hydration

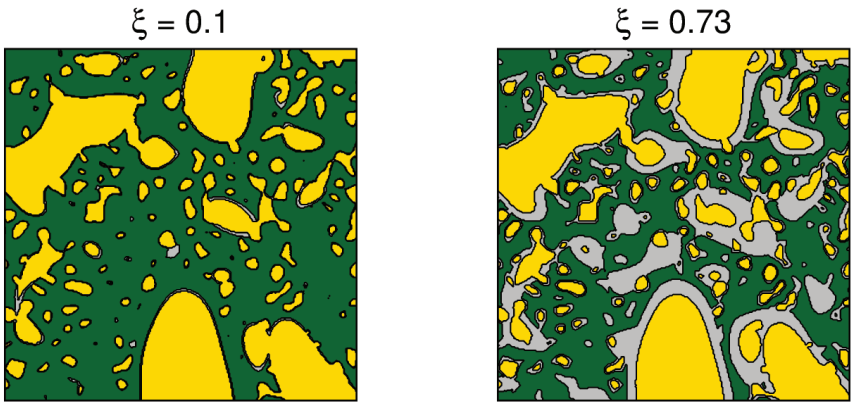

Figure 3. *Evolution of a selected morphology during hydration – $w/c = 0.4$, size T =100 µm (0.5 µm / pix) – Yellow: anhydrous cement, Green: water, Grey: hydration products*

model implementation allowing to take into account the mineralogical composition of the cement.

3. Calculation of the effective diffusivity of hydrated cement paste

In this section the interest of using the LBM is presented, in particular for effective diffusivity calculation in heterogeneous media. The aspects of the associated numerical stability are then reviewed. Eventually, the validation of the code versus an analytical solution and an example of result is presented.

3.1. *Diffusive transport in porous media*

Classically, the molecular diffusivity is given by Fick's law as per Equation [4], where D_j is the diffusivity of species j and c its concentration.

$$\frac{\partial c}{\partial t} = -D_j \nabla c \tag{4}$$

This formulation of diffusivity is valid locally on every phase j independently, which means it does not take into account the ionic interactions that may actually occur depending on the species diffusing in the considered materials (hence the *effective* diffusivity prediction, in contrast to the *apparent* one).

Regarding heterogeneous media, the homogenized effective diffusivity D_{eq} is calculated by applying a constant macroscopic concentration gradient between two opposite sides (based on Hill's criterion – Hill, (1963) – and the energy-dissipation equiv-

alence between scales), as in Ostoja-Starzewski & Schulte (1996). The macroscopic flux obtained by integration of the species flux on the boundaries (Pouya and Courtois (2002)) is then related to the effective diffusion coefficient.

3.2. *The Lattice Boltzmann Method*

The LBM is a mesoscopic approach for partial derivative equations problems. The evolution of a fluid or a solid is deduced from the consideration of a population of particles interacting with well-defined rules of collision. Unlike the well-known Navier-Stokes approach that uses the equations describing the macroscopic behaviour of a fluid and then discretizes them to the microscopic level, the LBM is an "ascendant" method, where the particles' agitation defined by the Maxwell-Boltzmann distribution of statistical mechanics allows for a consistent extrapolation towards the macroscopic behaviour. The link between micro and macroscopic scales is reached thanks to a Chapman-Enskog expansion (Wolf-Gladrow, 2000).

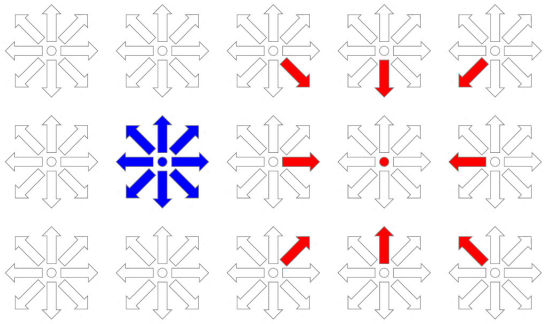

Figure 4. *D2Q9 Scheme - Arrows representing the possible directions of propagation of the distributions*

Practically, the LBM consists in considering a population of particles streaming along given directions in the space, systematically on the grid points. The particles' displacement is equal to unity in every direction, hence the time and space scales are strongly linked. At each time step, the particles' distributions stream orthogonally and diagonally to their neighbouring nodes and exchange their energy by collision. Figure 4 gives an example of distribution propagation for the D_2Q_9 model, where subscript "2" represents the dimension of space, "9" being the number of distributions streaming on the grid (8 possible space directions, plus the probability of staying on the same point).

Boltzmann's equation ruling the particles' behaviour is given under following form, f being the density of probability of the particles, c the speed of propagation and ω the collision operator:

$$\frac{\partial f}{\partial t} + c\nabla f = \Omega(f) \tag{5}$$

After discretizing the space into as previously defined, with a "lattice unit per time step in direction k" as the mesoscopic speed of the particle on the grid, one obtains:

$$\frac{\partial f_k}{\partial t} + c_k \frac{\partial f_k}{\partial dx} = \Omega_k \tag{6}$$

In the Bhatnagar-Gross-Krook approach (Nourgaliev et al. 2003), the collision operator is approximated as a relaxation of the distribution function towards the equilibrium distribution:

$$\Omega_k = -\frac{1}{\tau}(f_k - f_k^{eq}) \tag{7}$$

The equilibrium distribution function f_k^{eq} of Equation [7] is computed through the Taylor expansion of the Maxwell-Boltzmann distribution of a stationary perfect gas at the equilibrium, which simplifies for the diffusion process merely as Equation [7]:

$$f_k^{eq} = \omega_k \rho \tag{8}$$

The ρ factor in Equation [8] is simply the sum of the f_k distributions at the point considered and represents the computed macroscopic value, *e.g.* the concentration or temperature. The ω_k factor is a constant weighting relative to the propagation direction, such as $\sum_k \omega_k = 1$. Long displacements are less likely than short ones, hence the decreasing weightings of zero displacement, orthogonal displacement and diagonal displacement.

Setting $\omega = \Delta t/\tau$ out and writing the Boltzmann equation in its discrete form, one obtains the explicit equation of the space-time evolution of the functions:

$$f_k(x + \Delta x, t + \Delta t) = f_k(x, t) - \omega(f_k(x, t) - f_k^{eq}(x, t)) \tag{9}$$

For stability reasons of the LBM, the ω factor has to remain strictly between 0 and 2. In the case the case of two-dimensional diffusion in a single given medium, the relationship between ω and the "LBM diffusivity" d is as follows:

$$d = c_s^2(\frac{1}{\omega} - \frac{1}{2}) \tag{10}$$

In Equation [10], $c_s = 1/\sqrt{3}$ is a parameter called the sound speed in the LBM space-time, but is actually only a scaling factor in the case of diffusion (Nourgaliev et al. 2003, Servan-Camas et al. 2008). In order to make a LBM simulation with a given number of time steps and a mesh size with the evolution of a real domain , one has to make their Fourier numbers correspond:

$$F_o = \frac{d \times t_{LBM}}{N^2} = \frac{D \times t_{real}}{L^2} \tag{11}$$

Changing the "LBM diffusivity" or refining the mesh will hence affect the number of time steps to be computed. For more details about the LBM and its boundary conditions, please refer to Wolf-Gladrow (2000). Regarding the simulation of diffusion in two materials, the best practice is to define a relaxation factor for one of them and

then determine the value of the other one depending on the ratio of real diffusivities, as developed hereinafter: The phase "a" is considered as the reference phase (D_a, d_a) and is defined by its relaxation factor ω_a. The other phase must satisfy the relative ration between LBM and real worlds such as:

$$\frac{d_a}{d_b} = \frac{D_a}{D_b} \tag{12}$$

The other relaxation factor is hence given by following relationship:

$$\omega_b = (\frac{d_b}{c_s^2} + \frac{1}{2})^{-1} \tag{13}$$

The major interest of the LBM is its simple numerical implementation even for complex morphologies, the controlled change of the relaxation factor ω depending on the type of media considered on the regular grid allowing for a correct representation of the physics, without having to change the mesh at the interface. As we have seen, two parameters ω_a and ω_b have to be controlled in order ensure a consistent result, which will be detailed in following section.

3.3. *Numerical stability*

Another aspect of this study is the behaviour of the LBM-BGK algorithm depending on the variation of the relaxation factor ω, which affects the precision, computational cost and stability of the method. As mentioned in the previous section, the

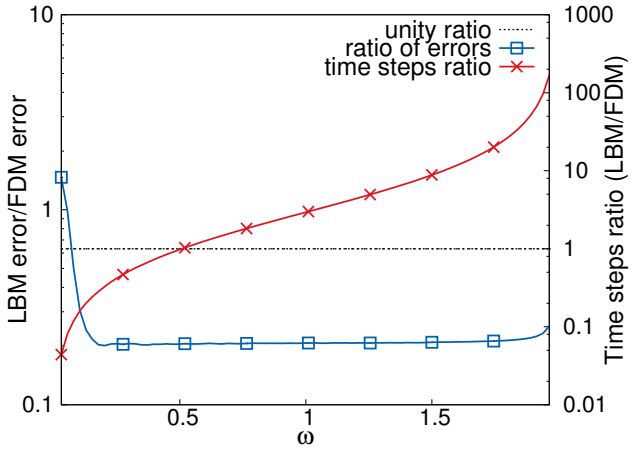

Figure 5. *Comparison of the LBM versus the finite-differences method for the diffusion problem*

relaxation factor depends on the LBM-diffusivity for a chosen problem. It also affects the computational cost, i. e. the number of time steps required to reach a given real

time and the precision of the method: taking the explicit Finite Differences Method (FDM) as a reference for comparison, one can see on Figure 5 the evolution of the error ratio between LBM and FDM, as well as the time steps ratio. The horizontal dotted line is the unity ratio for both methods' time steps and gives a measure of the time steps ratio required for the LBM compared to the explicit FDM. From Figure 5, one can conclude that the relaxation factor shall be small enough to be competitive versus classical methods, ideally below the unity ratio, yet big enough to allow for a sufficient precision of the method. The experience shows that for heterogeneous me-

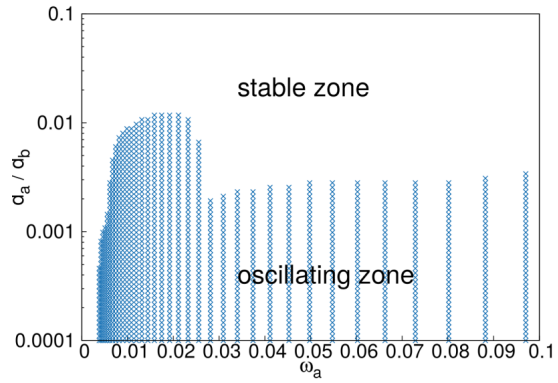

Figure 6. *Oscillating behavior for several diffusivity ratios depending on the relaxation factor*

dia with a diffusivity ratio reaching several orders of magnitude, some perturbations might appear at the interfaces between the phases. A numerical campaign of experiment allowed for the determination of the loci where no oscillations appear, as per Figure 6.

3.4. *Numerical results*

Theoretical aspects of the method being set, the validation of the model is developed in next section, followed by an application to diffusion in numerous morphologies of hydrated cement paste.

3.4.1. *Validation*

The effective diffusivity of the considered materials is assessed with the by summing all local contributions to yield the macroscopic equivalent flux. Mori & Tanaka's (1973) analytic approach of homogenization allows to verify the aptitude of the code to predict the equivalent diffusivity of a matrix with inclusions. Cylindrical, regular inclusions were put in the center of a matrix and the effective diffusivity was computed for different volume fractions of inclusion f_v and different diffusivity ratios d_a/d_b , resulting in a good accordance with Mori & Tanaka's reference scheme for this type

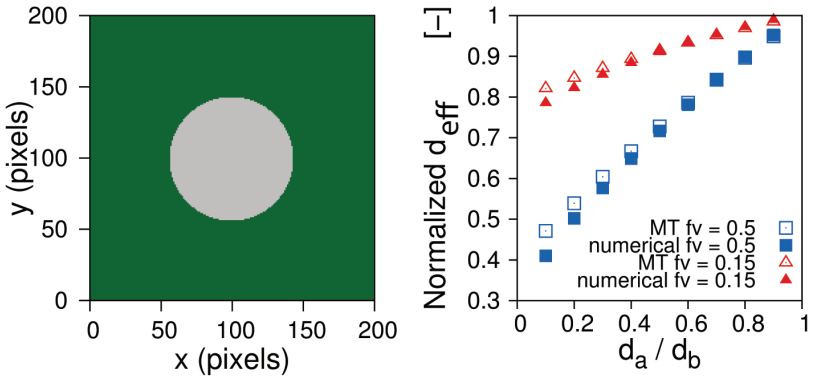

Figure 7. *Inclusion with $f_v = 15\%$ used for the benchmark (left) and results of the code validation versus Mori & Tanaka's analytical approach (right)*

of configurations, as presented on Figure 7, especially for diffusivity ratios close to unity (more details are given in Walther *et al.* (2014)).

3.4.2. *Cement paste application: Results*

In order to get a statistically representative description of hydrating cement paste, the level-set morphology reconstruction technique is used over 300 realizations of CRFs, for each degree of hydration. The hydrating cement paste microstructures (up to $100\times100\,\mu$m, with a resolution of $0.33\,\mu$m/pixel) are composed of water-saturated porosity (with a diffusive coefficient set to $D_w = 2.10^{-9}$ m^2/s), hydrates ($D_h = 2.10^{-12}$ m^2/s), and anhydrous cement. The latter being considered as a bulk matrix, thus non-diffusive. An example of the evolution of the morphology is shown Figure 3 where one can see two degrees of hydration. The effective diffusivity of cement paste with a w/c ratio of 0.4 is assessed during its hydration following the presented hydration framework.

3.4.2.1. RVE size for diffusion in cement pastes:

Several calculation were first done to assess a Representative Volume Element in regards to diffusion. In several numerical simulations (Zhang *et al.* (2011), Zhang *et al.* (2012) among others), the RVE is considered to be of size $T = 100\,\mu$m. Results for smaller morphologies are presented now, with intermediate microstructures of side size$16.6\,\mu$m, $33\,\mu$m, $66\,\mu$m and finally $100\,\mu$m. The discretization stays constant ($0.33\,\mu$m / pixel), and all presented results are averaged over 200 realizations. Size dependencie results are drawn Figure 8.

As the microstructures size increases, the value of the homogenized normalized effective diffusivity tends to stabilize. For the morphologies at $\xi = 0.1$, the effective diffusivity increases slightly with the microstrucure size, and the asymptotic value of diffusion coefficient is the one found in free water ; which was expected since nor

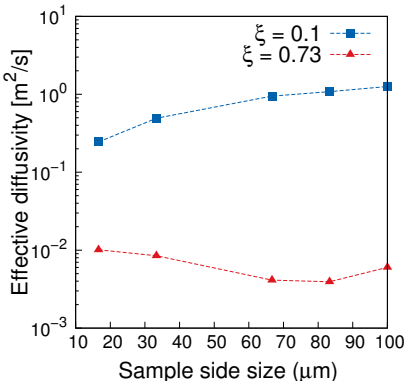

Figure 8. *Normalized diffusivity (with D_{pores} =1 $\mathrm{m}^2\,\mathrm{s}^{-1}$ and $D_{hydrates}/D_{pores} = 10^{-3}$) for various sizes of microstructure*

the inclusions or hydrates are percolated. It is only for sizes above $60\,\mu\mathrm{m}$ that the framework capture all the relevant morphological information (*e.g.* for smaller sizes, one could be simulating only a anhydrous residue, or a bulk hydrate with no porosity. For $\xi = \xi_{\max} = 0.73$, the results interpretations is less evident with first a decrease in terms of effective diffusivity, and then a slight increase.

In view of those results, and in the spirit of following the numerous previous attempts to simulates CP pastes morphologies, a side size of $100\,\mu\mathrm{m}$ is considered in the following.

3.4.2.2. Hydrating cement paste diffusivity:

The results in terms of averaged effective diffusivity are plotted on Figure 10 (and an example of a concentration distribution is shown Figure 9), with a 95% confidence interval for the 300 morphologies per hydration state. At the very beginning, the effective diffusivity is the one of water, which is in agreement with a well percolated pore-phase. Then, as the hydration evolves, the effective diffusivity decreases, with a significant change of slope around $\xi = 0.45$. This is due to the percolation of the hydrate's phase. Finally, the pore space is filled by the hydrates, and the effective diffusivity is closer to the hydrates one.

In addition, as the presented results are averaged over 300 realizations, the 95% confidence bounds are represented. They show an interesting feature as these bounds are slightly tighter for early hydration states as well as for final ones. At those states, one of the phases is "very" percolated (*i.e.* water is percolated or the hydrates are closing the diffusion paths - Figure 10 also illustrates this behavior), and thus the macroscopic response depends first on this phase properties. On the other hand, in the vicinity of the change of slope those bounds are looser, as there is no predominant percolated phase, and morphological variability is higher.

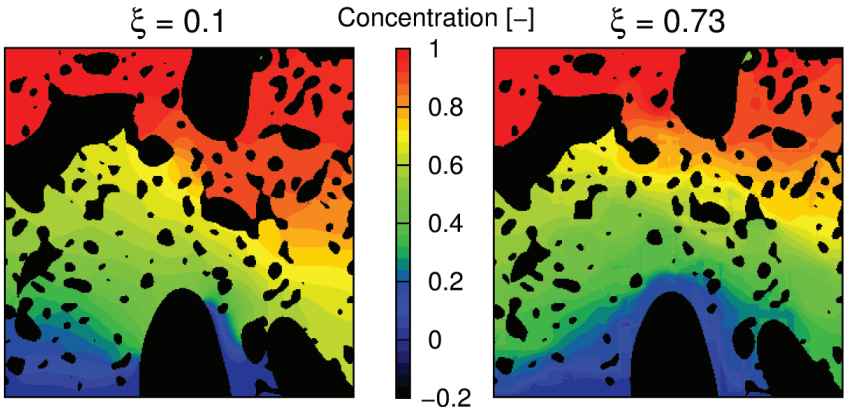

Figure 9. *Concentration distribution in steady state under a unitary concentration gradient* – $w/c = 0.4$, *size* $T = 100\,\mu\text{m}$ *(*$0.5\,\mu\text{m}$ */ pix)*

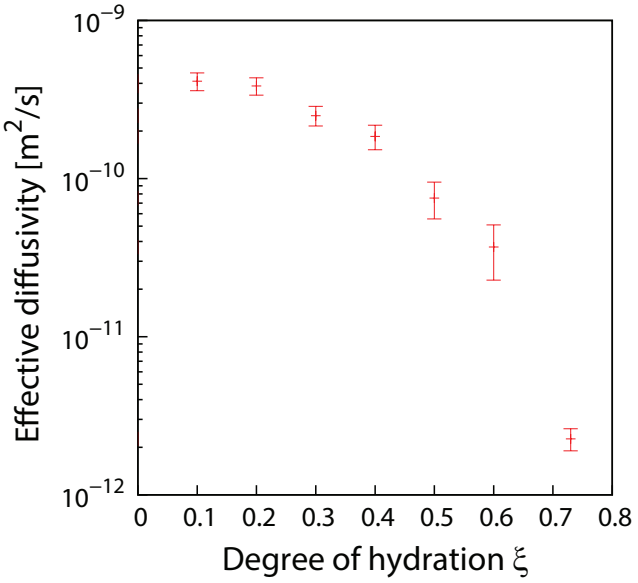

Figure 10. *Simulated average effective diffusivity of standard cement paste* ($w/c = 0.4$ – $\xi \in [0; \xi_{max}]$) *with 95% confidence intervals*

4. Conclusions

This study presents a method for creating hydrating cement paste morphologies thanks to the level-set method.Through its explicit formulation and regular meshing,

the LBM offers a simple implementation which is of interest for the calculation of the effective diffusivity of heterogeneous media having a strong variability of diffusive properties over time.

Future developments of this work include the extension of the LBM model to 3D, allowing for a proper comparison with experimental results. The tortuosity and pore connectivity in three dimensions are indeed very different than the two-dimensional ones. As they play a major role in transport properties, we expect the effective diffusivity to change significantly. This will allow to compare the 2D and 3D modeling approaches, and possibly to find a link to reduce even further the computational costs of the effective properties predicting framework (Qiao, 2012). The calculation of instantaneous diffusion properties of cement paste during hydration (*id est* changing morphology), as well as including the effects of other chemical species in presence shall also be included in the model.

5. Bibliographie

[Adler, 2008] ADLER R., "Some new random field tools for spatial analysis ", *Stochastic Environmental Research and Risk Assessment*, vol. 22, num. 6, p. 809-822, Sep. 2008

[Bogdan *et al.*, 2014] BOGDAN M., BENBOUDJEMA F. COLLIAT J.-B., STEFAN L. "Microscopic model for concrete diffusivity predictions" *Conference proceedings, EURO-C 2014: Computational Modelling of Concrete and Concrete Structures*, vol. 2, p. 667–678

[van Breugel 1991] VAN BREUGEL K., "Simulation of hydration and formation of structure in hardening cement-based materials", PhD Thesis, Delft University of Technology, Delft, 1991

[Bentz, 1991] BENTZ D.P. , GARBOCZI B. , "Digital-image-Based computer modeling of cement-based materials", *Digital Image Processing: Techniques and Application in Civil Engineering*, 1993

[Hill, 1963] HILL, R., "Elastic properties of reinforced solids: Some theoretical principles", *Journal of Mechanics and Physics of Solids*, vol. 11 1963

[Jennings & Tennis, 1994] JENNINGS, H. , TENNIS, P., "Model for the developing microstructure in Portland cement pastes", *Journal of the American Ceramic Society*, vol. 77 1994

[Mohamad, 2007] MOHAMAD A. A. " Applied Lattice Boltzmann Method for Transport Phenomena, Momentum, Heat & Mass Transfer", second ed., Dept. of Mechanical and Manufacturing Engineering, University of Calgary: Schulich School of Engineering. 2007

[Mori & Tanaka, 1973] MORI T., TANAKA K. " Average stress in matrix and average elastic energy of materials with misfiting inclusions", *Acta Metallurgica*, 21, 571-574. 1973

[Nourgaliev *et al.*, 2003] NOURGALIEV R.R., DINH T.N., THEOFANOUS T.G., JOSEPH D. " The lattice Boltzmann equation method : theoretical interpretation, numerics and implications", *International Journal of Multiphase Flow*, 29, 117-169. 2003

[Ostoja-Starzewski & Schulte, 1996] OSTOJA-STARZEWSKI, M. SCHULTE, J. " Bounding of effective thermal conductivities of multiscale materials by essential and natural boundary conditions. ", *Physical review B*, 54, 1669

[Pouya & Courtois, 2002] POUYA A., COURTOIS A. " Définition de la perméabilité équivalente des massifs fracturés par des méthodes d'homogénéisation ", *C.R. Earth and Planetary Science*, 334, 975-979. 2002

[Powers, 1947] POWERS T.C., BROWNYARD T.L., "Studies of the physical properties of hardened Portland cement paste", *Research Laboratories of the Portland Cement Paste*, vol. 22, Chicago, 1947

[Qiao, 2012] QIAO, J., "Modélisation des propriétés thermomécaniques effectives de dépôts élaborés par projection thermique", PhD Thesis, Université de Technologie de Belfort-Montbeliard, FRANCE, 2012

[Roubin *et al.*, 2015] ROUBIN E., COLLIAT J.-B., BENKEMOUN N., , "Meso-scale modeling of concrete: A morphological description based on excursion sets of Random Fields.", *Computational Materials Science* vol. 102, 2015

[Servan-Camas & Sai, 2008] SERVAN-CAMAS B., SAI F.T.C. " Non-negativity and stability analyses of Lattice-Boltzmann Method for advection-diffusion equation ", *Journal of Computational Physics*, 228 (1), 236-256. 2008

[Walther *et al.*, 2014] WALTHER E., DESA C., BENNACER R. " Lattice Boltzmann Method Applied to Diffusion in Restructured Heterogeneous Media", *Defect and Diffusion Forum*, 354, 237-242. 2014

[Wolf-Gladrow, 2000] WOLF-GLADROW D.A. " Lattice-Gas Cellular automata and Lattice Boltzmann Models - An Introduction ", Springer. 2000

[Zhang *et al.* 2011] ZHANG M. , YE G. , VAN BREUGEL K., "Lattice Boltzmann simulation of the ionic diffusivity of cement paste", International RILEM Conference on Advances in Construction Materials Through Science and Engineering, pp.1-9, 2011.

[Zhang *et al.* 2012] ZHANG M. , YE G. , VAN BREUGEL K., "Modeling of ionic diffusivity in non-saturated cement-based materials using lattice Boltzmann method", Cement and Concrete Research 42(11), pp.1524-1533, 2012.